Published in final edited form as:

Adv Funct Mater. 2017 February 23; 27(8): . doi:10.1002/adfm.201604671.

Neuroendocrine Tumor-Targeted Upconversion Nanoparticle-Based Micelles for Simultaneous NIR-Controlled Combination Chemotherapy and Photodynamic Therapy, and Fluorescence Imaging

Guojun Chen,
Department of Materials Science and Engineering, University of Wisconsin–Madison, Madison, WI 53715, USA. Wisconsin Institute for Discovery, University of Wisconsin–Madison, Madison, WI 53715, USA

Prof. Renata Jaskula-Sztul,
Department of Surgery, University of Alabama at Birmingham, Birmingham, AL 35233, USA

Corinne R. Esquibel,
Laboratory for Optical and Computational Instrumentation, University of Wisconsin–Madison, Madison, WI 53706, USA

Irene Lou,
Department of Surgery, University of Wisconsin–Madison, Madison, WI 53705, USA

Qifeng Zheng,
Department of Materials Science and Engineering, University of Wisconsin–Madison, Madison, WI 53715, USA. Wisconsin Institute for Discovery, University of Wisconsin–Madison, Madison, WI 53715, USA

Ajitha Dammalapati,
Department of Surgery, University of Wisconsin–Madison, Madison, WI 53705, USA

April Harrison,
Department of Surgery, University of Wisconsin–Madison, Madison, WI 53705, USA

Prof. Kevin W. Eliceiri,
Wisconsin Institute for Discovery, University of Wisconsin–Madison, Madison, WI 53715, USA. Department of Biomedical Engineering University of Wisconsin–Madison, Madison, WI 53706, USA. Laboratory for Optical and Computational Instrumentation, University of Wisconsin–Madison, Madison, WI 53706, USA

Prof. Weiping Tang,
School of Pharmacy, University of Wisconsin–Madison, WI 53705, USA

Prof. Herbert Chen, and
Department of Surgery, University of Alabama at Birmingham, Birmingham, AL 35233, USA

Correspondence to: Herbert Chen; Shaoqin Gong.

Supporting Information

Supporting Information is available from the Wiley Online Library or from the author.

Prof. Shaoqin Gong
Department of Materials Science and Engineering, University of Wisconsin–Madison, Madison, WI 53715, USA. Wisconsin Institute for Discovery, University of Wisconsin–Madison, Madison, WI 53715, USA. Department of Biomedical Engineering University of Wisconsin–Madison Madison, WI 53706, USA

Abstract

Although neuroendocrine tumors (NETs) are slow growing, they are frequently metastatic at the time of discovery and no longer amenable to curative surgery, emphasizing the need for the development of other treatments. In this study, multifunctional upconversion nanoparticle (UCNP)-based theranostic micelles are developed for NET-targeted and near-infrared (NIR)-controlled combination chemotherapy and photodynamic therapy (PDT), and bioimaging. The theranostic micelle is formed by individual UCNP functionalized with light-sensitive amphiphilic block copolymers poly(4,5-dimethoxy-2-nitrobenzyl methacrylate)-polyethylene glycol (PNBMA-PEG) and Rose Bengal (RB) photosensitizers. A hydrophobic anticancer drug, AB3, is loaded into the micelles. The NIR-activated UCNPs emit multiple luminescence bands, including UV, 540 nm, and 650 nm. The UV peaks overlap with the absorption peak of photocleavable hydrophobic PNBMA segments, triggering a rapid drug release due to the NIR-induced hydrophobic-to-hydrophilic transition of the micelle core and thus enabling NIR-controlled chemotherapy. RB molecules are activated via luminescence resonance energy transfer to generate $^1O_2$ for NIR-induced PDT. Meanwhile, the 650 nm emission allows for efficient fluorescence imaging. KE108, a true pansomatostatin nonapeptide, as an NET-targeting ligand, drastically increases the tumoral uptake of the micelles. Intravenously injected AB3-loaded UCNP-based micelles conjugated with RB and KE108—enabling NET-targeted combination chemotherapy and PDT—induce the best antitumor efficacy.

1. Introduction

Neuroendocrine tumors (NETs), such as medullary thyroid cancers, carcinoids, islet cell tumors, and small cell lung cancers, frequently metastasize to the liver.[1] Unfortunately, patients with isolated NE liver metastases have poor survival outcomes.[1c,2] Furthermore, patients with NETs often have debilitating symptoms, such as uncontrollable diarrhea, skin rashes, flushing, and heart failure due to excessive hormone secretions,[3] thus leading to a poor quality of life. While surgical resection can be potentially curative, many patients are not candidates for operative intervention due to widespread metastases. Moreover, other forms of therapy, including chemoembolization, radioembolization, radiofrequency ablation, and cryoablation, have had limited efficacies.[3a,4] Therefore, besides surgery, there are no curative treatments for NETs and their hepatic metastases. However, even surgical resection is often followed by disease recurrence, thereby emphasizing the need for the development of other forms of therapy.

Nanotheranostics, the integration of diagnostic and therapeutic capabilities into one nanoplatform, may enable simultaneous imaging and therapy, thereby making personalized medicine possible. Nanotheranostics are of great interest for targeted cancer theranostics for the following reasons. (1) Nanoparticles (NPs) with high surface-to-volume ratios can offer

high loading capacities for multiple payloads, including anticancer agents (e.g., drugs, peptides, genes, etc.), imaging probes (e.g., dyes, radioisotopes, etc.), and tumor-targeting ligands (e.g., small molecules, peptides, antibodies, aptamers, etc.).[5] (2) NPs can effectively deliver these payloads to tumor lesions due to their passive (via the enhanced permeability and retention (EPR) effect) and active (via cell-specific ligand conjugation) tumor-targeting abilities.[6] (3) NPs can deliver multiple agents simultaneously, thus enabling combination therapies, such as chemotherapy and photodynamic therapy (PDT), which can significantly enhance their therapeutic indexes.[7]

Photodynamic therapy (PDT) is clinically approved and known as a minimally invasive medical technology for neo-plastic disease treatment.[8] PDT was the first drug–device combination approved by the U.S. Food and Drug Administration (FDA) two decades ago.[8] Typically, it involves three key components: photosensitizer, light, and tissue oxygen.[8,9] Upon excitation of the photosensitizer under lights with proper wavelengths, the photosensitizer is able to transfer the absorbed photon energy to the oxygen molecules in the surroundings, thereby generating cytotoxic singlet oxygen ($^1O_2$) to kill cancer cells. PDT can provide high specificity for the treatment of particular lesions through the control of light exposure to the photosensitizer, thereby minimizing any potential detrimental side effects on normal tissues.[9,10] However, one major limitation with current PDT is its relatively low tissue penetration depth since most photosensitizers are excited by visible or even UV light, thus limiting its applications.[11] Near-infrared (NIR) light in the range of 700–1100 nm, known as the optical tissue penetration window, can penetrate deeper into biological tissues than UV or visible light and thus is ideal for phototherapies including PDT and optical imaging.[11]

Lanthanide ion (Ln^{3+}, such as Er^{3+}, Tm^{3+}, Yb^{3+})-doped upconversion nanoparticles (UCNPs) have attracted much attention in recent years for biomedical applications due to their unique ability of converting NIR light to higher-energy photons (e.g., UV and visible light).[11b,c,12] Therefore, photosensitizers attached to lanthanide-doped UCNPs can be activated by NIR light via resonance energy transfer to effectively generate cytotoxic $^1O_2$.[13] Photosensitizers can be loaded onto the UCNPs either via physical adsorption or chemical conjugation. Physical adsorption is less desirable due to the high possibility of desorption and/or leakage of the photosensitizers from the UNCPs, resulting in low/limited efficacies.[11c,12a,b,14] Conjugating photosensitizers onto UCNPs via covalent bonds can effectively overcome this limitation and thus is more desirable for UCNP-based PDT.[12b,14b,15] In contrast to “free” photosensitizers employed by traditional PDT that are subject to fast clearance and lack tumor-targeting abilities, conjugating photosensitizers onto UCNPs can also effectively increase the accumulation of photosensitizers in the target tumor tissues/cells due to the unique tumor-targeting abilities of the nanoparticles.

It has been demonstrated recently that UCNP-based combination chemotherapy and PDT can lead to much better therapeutic outcomes than chemotherapy or PDT alone.[16] However, these previous studies either did not carry out any in vivo studies, only investigated the anticancer efficacy of intratumorally injected nanoparticles, or used a relatively high laser power density (e.g., 2.5 W cm^{-2}).[16] In this study, we developed a unique NET-targeting UCNP-based micelle capable of NIR-controlled combination

chemotherapy and PDT, as well as fluorescence imaging (Scheme 1A) and studied their in vivo tumor targeting behavior and anticancer efficacy in NET-bearing mice through intravenous injection. The laser power density used for this study was 500 mW cm^{-2}, which is well below the conservative limit of 980 nm laser intensity (726 mW cm^{-2}) for biological studies and clinical applications.[17] The following four factors were taken into consideration for the design of this multifunctional UCNP-based nanoplatform. (1) UCNPs can offer high-quality imaging due to their low background autofluorescence.[12b,18] (2) Covalent conjugation of photosensitizers onto the UCNPs can enable a more efficient NIR-activated PDT. (3) NIR-controlled fast drug release at tumor sites can potentially enhance the therapeutic efficacy of chemotherapy. (4) KE108 peptide, a true pansomatostatin synthetic nonapeptide, can potentially serve as an effective tumor targeting ligand for medullary thyroid cancers, a common type of NETs.

More specifically, the $NaYF_4$:Yb/Tm/Er UCNPs emitted light in the UV, visible, and far-red regions. The far-red emission (650 nm) of the UCNPs was employed for the UCNP-based theranostic micelle imaging in vitro and in vivo. Rose Bengal (RB) photosensitizer molecules were covalently conjugated onto the UCNP core. Since the UCNP's luminescence band around 540 nm overlapped with the absorption peak of RB, RB molecules were activated via resonance energy transfer by the NIR-activated UCNPs to effectively generate $^1O_2$ for PDT. As shown in Scheme 1B, the hydrophobic core of the UCNP-based theranostic micelle was formed by a photosensitive poly(4,5-dimethoxy-2-nitrobenzyl methacrylate) (PNBMA) polymer that can undergo a hydrophobic-to-hydrophilic transition under the UV light emitted by NIR-activated UCNPs due to photo induced polymer side-group cleavage. The NIR-triggered hydrophobic-to-hydrophilic transition of the micelle core subsequently caused a rapid release of the encapsulated hydrophobic drug (e.g., AB3, a histone deacetylase (HDAC) inhibitor whose chemical structure is shown in Figure S1, Supporting Information), thus leading to superior anticancer efficacy.[19] Finally, the UCNP-based theranostic micelles were also conjugated with KE108 peptide, an NET-targeting ligand, which can specifically and efficiently target all five subtypes of somatostatin receptors (SSTRs) overexpressed by NET cells. We have recently demonstrated that KE108 possesses superior tumor targeting abilities in carcinoid xenograft animal models over other commonly used somatostatin analogs, such as octreotide.[20] Our studies have demonstrated that NIR-controlled combination chemotherapy and PDT enabled by these unique UCNP-based theranostic micelles administered intravenously were very effective in suppressing the tumor growth of medullary thyroid cancer. We have also shown that these UCNP-based theranostic micelles can effectively serve as imaging probes specifically targeting the medullary thyroid tumors (Scheme 1C).

2. Results and Discussion

2.1. Synthesis and Characterization of UCNP-Based Theranostic Micelles

The $NaYF^4$:Yb^{3+}/Er^{3+}/Tm^{3+} UCNP core was first prepared using a thermal decomposition method in oleylamine.[12b] The hydrophilic amino-functionalized UCNPs (NH_2-UCNPs) were synthesized via a ligand-exchange approach using 2-aminoethyl dihydrogenphosphate (AEP) as a surface coating agent to replace the original oleylamine ligand. The crystal

structure of the $NaYF_4$:Yb^{3+}/Er^{3+}/Tm^{3+} UCNPs and the presence of elements including Na, F, Y, Yb, Er, and Tm in these UCNPs was characterized by X-ray diffraction (XRD) (Figure S2A, Supporting Information) and energy-dispersive X-ray (EDX) spectroscopy (Figure S2B, Supporting Information), respectively. The Fourier transform infrared (FTIR) absorption spectra shown in Figure 1A confirmed the successful coating of AEP on the surface of the UCNPs. The two new absorption bands around 1115 and 1014 cm^{-1} were attributed to the O=P stretching vibration mode and P–O–C vibration mode, respectively. Meanwhile, the long alkyl chain (–(CH_2))–, $n > 4$) vibration mode located at 736 cm^{-1} attributed to oleylamine disappeared after ligand exchange. The average size of the NH_2-UCNPs determined by transmission electron microscopy (TEM) was around 14 nm in diameter (Figure 1B). The photosensitizer RB and the alkyne functional groups (dibenzocyclooctyne acid, DBCO) were conjugated onto the UCNPs via an amidation reaction to form RB/alkyne-UCNPs. The photosensitive amphiphilic block copolymers polyethylene glycol (PEG)-PNBMA-N_3 and KE108-PEG-PNBMA-N_3 were prepared by atom transfer radical polymerization (ATRP) (detailed characterization can be found in the Supporting Information, Figure S3 and Table S1, Supporting Information) and then conjugated onto the RB/alkyne-UCNPs via catalyst-free click chemistry,[21] as shown in Figure 2.

Figure 3A (black line) shows the luminescence emissions of the NH_2-UCNP upon 980 nm excitation, including UV light (340–370 nm), 460, 540, and 650 nm. The red line in Figure 3B represents the UV–vis absorption spectrum of the resulting UCNP-RB/PNBMA-PEG nanoparticles. The strong absorption peaks at the UV region are attributed to the hydrophobic PNBMA blocks, which can form a hydrophobic micelle core wherein hydrophobic drugs can be encapsulated. As reported previously, when excited by UV light, the hydrophobic PNBMA segments can undergo a hydrophobic-to-hydrophilic transition, resulting from the cleavage of the *o*-nitrobenzyl groups on the PNBMA chain, as indicated in Scheme 1B. Hence, upon NIR activation, the UCNP would emit UV light, which would subsequently trigger a hydrophobic-to-hydrophilic transition of the micelle core formed by the PNBMA, thereby inducing a rapid drug release as described in detail later. Changes in the chemical structure of the PNBMA polymer segments after 980 nm laser illumination (10 min; 0.5 W cm^{-2}) were confirmed by ^1H NMR as shown in Figure S4 (Supporting Information). The peaks ascribed to *o*-nitrobenzyl groups were significantly decreased after 980 nm laser irradiation for 10 min. The absorbance of the RB photosensitizers also overlapped with the 540 nm luminescence emission of the UCNPs under 980 nm irradiation, thereby enabling NIR-controlled PDT via luminescence resonance energy transfer as discussed later. RB is a photosensitizer with a proven record for producing singlet oxygen with high yields.[22] In this study, ≈100 RB molecules were conjugated per UCNP in order to effectively generate singlet oxygen.[12b] Furthermore, the far-red luminescence emission at 650 nm of the NIR-activated UCNPs was conveniently used for fluorescence imaging in vitro and in vivo.

The individual UCNP functionalized with amphiphilic block copolymer PNBMA-PEG and RB (i.e., UCNP-RB/PNBMA-PEG) can form a stable micelle in an aqueous solution due to its globular structure as well as a large number of amphiphilic arms with a proper hydrophobic-to-hydrophilic ratio.[23] The morphologies of the UCNP-based theranostic

micelles were studied by dynamic light scattering (DLS) and TEM. As shown in Figure 3B, the average hydrodynamic diameter of the UCNP-based micelles was 39 nm (PDI = 0.11). The TEM image of the UCNP-based micelles (Figure 3C) showed a spherical morphology with an average diameter of around 29 nm. The size range of the UCNP-based theranostic micelles is suitable for targeted cancer theranostics.[24] AB3 was loaded into the hydrophobic core of the micelles by a dialysis method[23c] and the AB3 loading level was 16.7 wt%.

2.2. NIR-Controlled In Vitro Drug Release

Light-controlled drug release has been reported previously.[25] However, in most cases, high-energy UV or at least visible light, offering a limited tissue penetration depth, is required. NIR light is preferred since it provides a greater tissue penetration depth and is less detrimental to healthy cells.[7a] In this study, taking advantage of the UV luminescence emission of NIR (980 nm)-activated UCNPs, the photosensitive hydrophobic PNBMA segments underwent a hydrophobic-to-hydrophilic transition, thereby causing a faster release of the hydrophobic drug AB3 (an HDAC inhibitor), which was originally encapsulated into the hydrophobic PNBMA core of the micelles mainly through hydrophobic interactions. As shown in Figure 4A, without the 980 nm laser, only a small portion of the drug (<14 wt%) was released after 16 h. However, after 10 min irradiation with a 980 nm laser (0.5 W cm^{-2}), the rate of drug release increased drastically, and nearly 75 wt% drug was released after 16 h. It has been demonstrated that the faster release of chemoagents in target tumors leads to better chemotherapies,[19] which is consistent with our findings (presented in the *In Vivo Anticancer Study* section). Hence, this NIR-controlled drug release behavior makes this UCNP-based theranostic micelle a very promising drug delivery nanoplatform.

2.3. NIR-Triggered $^1O_2$ Generation

Generation of cytotoxic $^1O_2$ is critical in photodynamic cancer cell killing. The efficiency of $^1O_2$ generation by RB-conjugated UCNP-based micelles under 980 nm laser irradiation was studied using a standard protocol by monitoring the absorption intensity of 1,3-diphenylisobenzofuran (DPBF).[26] DPBF is a commonly used agent to detect $^1O_2$. It can react with singlet oxygen irreversibly and thus causes a decrease in the intensity of DPBF absorption at 417 nm. In this study, three systems were tested, namely, free RB and UCNP-based micelles with or without RB conjugation. As shown in Figure 4B, there was no DPBF consumption in those three systems without NIR irradiation, thus indicating that no $^1O_2$ was generated. Similarly, for free RB and UCNP-based micelles without RB conjugation, no sign of $^1O_2$ generation was observed under 980 nm laser irradiation. However, for the RB-conjugated UCNP-based micelles, DPBF was clearly consumed upon 980 nm laser irradiation, hence demonstrating the generation of $^1O_2$. Moreover, the amount of $^1O_2$ generated increased with the NIR irradiation time since more DPBF was depleted. Taken together, cytotoxic $^1O_2$ can be effectively generated by RB-conjugated UCNPs under NIR light irradiation, thereby enabling NIR-induced PDT.

2.4. Cellular Uptake Study Using Multiphoton Fluorescence Microscopy Based on the 650 nm Luminescence Emission of NIR-Activated UCNPs

The far-red 650 nm luminescence emission of UCNPs under 980 nm excitation was utilized for micelle detection. NET cells often overexpress SSTRs.[20,27] KE108 peptide, a somatostatin analog that can bind efficiently to all five subtypes of SSTRs, was conjugated to the digital end of the PEG blocks as an NET-targeting ligand. TT cells (human medullary thyroid cancer cell line, a type of NET cells; the SSTR expression levels are shown in Figure S5, Supporting Information) were treated with either pure medium (i.e., control), UCNP-based micelles (i.e., nontargeted), KE108-conjugated UCNP-based micelles (i.e., targeted), or KE108-conjugated UCNP-based micelles together with free KE108 peptide (i.e., the blocking assay). As shown in Figure 5A, the 650 nm emission (red color) of UCNP under 980 nm excitation was detected using a multiphoton microscope. Furthermore, a much higher red intensity was observed clearly in cells treated with targeted micelles compared to those treated with nontargeted micelles, demonstrating that the KE108 peptide can effectively enhance the cellular uptake of micelles through a receptor-mediated endocytosis process. On the contrary, in the blocking experiment, when the SSTRs on the TT cells were saturated by free KE108 peptides, the level of cellular uptake of targeted micelles was comparable to that of the nontargeted micelles. The targeting ability of KE108 peptide was further confirmed by flow cytometry analyses (Figure S6, Supporting Information) based on the fluorescence of RB. Taken together, these results confirmed the capability of UCNP-based micelles for bioimaging, as well as the excellent SSTR-targeting ability of the KE108 peptide.

2.5. In Vitro Combination Chemotherapy and PDT Using AB3-Loaded and RB-Conjugated UCNP-Based Micelles

Encouraged by the capabilities of the NIR-triggered fast drug release and the efficient generation of cytotoxic $^1O_2$ by the UCNP-based micelles, we tested the efficacy of combination chemotherapy and PDT on TT cells in vitro. The cells were divided into twelve treatment groups (abbreviations for all treatment groups were summarized in Table 1) with or without 980 nm laser illumination: free RB, AB3, AB3+RB, blank UCNP-based nontargeted micelles (NT), blank UCNP-based targeted micelles (T), RB-conjugated UCNP-based nontargeted micelles (NT-RB), RB-conjugated UCNP-based targeted micelles (T-RB), AB3-loaded UCNP-based nontargeted micelles (NT-AB3), AB3-loaded UCNP-based targeted micelles (T-AB3), AB3-loaded and RB-conjugated UCNP-based nontargeted micelles (NT-RB-AB3), and AB3-loaded and RB-conjugated UCNP-based targeted micelles (T-RB-AB3). As shown in Figure 5B, free RB and blank UCNP-based micelles did not cause any cell deaths with or without laser treatment. Without laser illumination, neither NT-RB nor T-RB showed any PDT effect and no $^1O_2$ was produced. However, under 980 nm laser illumination (0.5 W cm^{-2} for 10 min), about 18% and 26% cell death was observed for cells treated with NT-RB and T-RB for 48 h, respectively, thus demonstrating the effectiveness of PDT. The increased cytotoxicity of T-RB over NT-RB was attributed to the enhanced cellular uptake of the targeted micelles via receptor-mediated endocytosis, as discussed earlier. The viability of cells treated with pure AB3 with or without laser treatment was 56% and 54%, respectively, suggesting that 980 nm laser irradiation for 10 min did not notably affect the cell viability of pure AB3. Treatment with AB3-loaded UCNP-based

micelles (without any RB conjugation), without 980 nm laser irradiation, resulted in a 20% (NT-AB3) and 42% (T-AB3) cancer cell death, whereas under 980 nm laser irradiation, the percentage of cell death increased to 32% (NT-AB3) and 53% (T-AB3), respectively. The higher cytotoxicity observed in the laser groups was ascribed to the NIR-triggered fast AB3 drug release.[19] Meanwhile, the increased cytotoxicity in targeted groups over nontargeted groups was attributed to the enhanced cellular uptake of micelles through SSTR-mediated endocytosis. More importantly, 86% cell death was observed for cells treated with T-RB-AB3 (last bar) under 980 nm laser irradiation due to a combination of chemotherapy and PDT, which provided a dramatically better therapeutic index than chemotherapy alone (T-AB3, 53% cell death) or PDT alone (T-RB, 31% cell death). Similarly, the T-RB-AB3-Laser treatment (86% cell death) induced higher cytotoxicity over the NT-RB-AB3-Laser (59% cell death) because the KE108 targeting ligand significantly enhanced the cellular uptake of the micelles.

2.6. Tumor Accumulation of UCNP-Based Micelles

As aforementioned, UCNPs emitting the far-red 650 nm luminescence under 980 nm light excitation served as an excellent imaging probe in vivo.[28] Herein, the in vivo tumor accumulation of the UCNP-based micelles was investigated in TT-tumor-bearing mice. The mice were intravenously injected with saline (control), nontargeted micelles (i.e., UNCP-based micelles without KE108 conjugation), and targeted micelles (i.e., KE108-conjugated UCNP-based micelles). Five hours postinjection, the mice were analyzed using a multiphoton microscope (Ex/Em: 980/650 nm). As shown in Figure 6, no far-red signal was detected in the control group. However, red luminescence (650 nm) was clearly visible in both the nontargeted group and targeted group upon 980 nm excitation. Moreover, a much stronger micelle signal was observed in the mice treated with targeted micelles, demonstrating the excellent in vivo targeting ability of the KE108 peptide. In contrast to nontargeted micelles that only exhibit passive tumor-targeting ability via the enhanced permeation and retention (EPR) effect, KE108-conjugated (i.e., targeted) micelles possessed both passive and active NET targeting abilities, thereby leading to a significantly higher micelle tumor accumulation. Ex vivo imaging of the excised tumors (Figure S7, Supporting Information; based on the RB fluorescence) further confirmed the greater tumor uptake of the targeted micelles compared to the nontargeted ones.

The NET targeting and in vivo imaging capabilities of the UCNP-based theranostic micelles were also studied in a TT-liver-metastases mouse model. The intrasplenic injections of human TT cells were described in detail in the Experimental Section. Six weeks post-intrasplenic injection, mice were intravenously injected with targeted micelles. We have shown that the KE108-conjugated UCNP-based micelles targeted the liver metastases nodules very effectively, and emissions at 650 nm from the NIR-activated UCNP-based micelles were detected mostly within the tumor metastases (Figure S8, Supporting Information). This study has demonstrated that nanoparticle with KE108 as the active targeting ligand can effectively target NET-liver-metastases, which warrants further studies in the future.

2.7. In Vivo Anticancer Efficacy of the Combination Chemotherapy and PDT

To assess the therapeutic efficacy of UCNP-based micelles, a subcutaneous TT-tumor xenograft mouse model was used. When mice developed palpable tumors, they were intravenously injected with one of the following ten agents: saline (control), pure AB3, RB-conjugated targeted micelles with or without laser (i.e., T-RB-Laser or T-RB), AB3-loaded targeted micelles with or without laser (i.e., T-AB3-Laser or T-AB3), AB3-loaded nontargeted micelles with or without laser (i.e., NT-RB-AB3-Laser or NT-RB-AB3), and AB3-loaded targeted micelles with or without laser (i.e., T-RB-AB3-Laser or T-RB-AB3) at Day 0 and Day 7, at an equivalent AB3 dosage of 30 mg kg^{-1} BW, which is below the maximum tolerated dose (MTD, 50 mg kg^{-1} BW). All laser treatments were conducted by applying a continuous wave fiber-coupled 980 nm laser (0.5 W cm^{-2}, 15 min, 1 min interval after each 5 min of irradiation) at tumor sites 4 h postinjection. Changes in relative tumor volume are shown in Figure 7A. T-AB3 (final tumor volume: 778.8 ± 57.9 mm^3) exhibited a better anticancer efficacy than pure AB3 (final tumor volume: 1160.2 ± 89.2 mm^3; $p < 0.01$), thus demonstrating the benefit of using targeted drug nanocarriers. Moreover, T-AB3-Laser (final tumor volume: 625.8 ± 40.7 mm^3; NIR-controlled chemotherapy) showed a better outcome than T-AB3 without laser (final tumor volume: 778.8 ± 57.9 mm^3; $p < 0.05$), resulting from the faster drug release triggered by the NIR light.[19] Meanwhile, T-RB (final tumor volume: 1463.2 ± 140.6 mm^3) did not exhibit any therapeutic effect without the 980 nm illumination, as compared to the control group (final tumor volume: 1557.2 ± 163.6 mm^3). In contrast to this experiment, tumor exposure to NIR light (T-RB-Laser) resulted in a significant anticancer effect (final tumor volume: 872.6 ± 63.0 mm^3; NIR-controlled PDT; $p < 0.01$) due to NIR-activated PDT. Furthermore, T-RB-AB3-Laser (final tumor volume: 171.3 ± 13.7 mm^3), which enabled combination chemotherapy and PDT, produced a much better anticancer efficacy than either chemotherapy alone (T-AB3-Laser; final tumor volume: 625.8 ± 40.7 mm^3; $p < 0.001$) or PDT alone (T-RB-Laser; final tumor volume: 872.6 ± 63.0 mm^3; $p < 0.001$). Moreover, the T-RB-AB3-Laser showed much better anticancer efficacy than the NT-RB-AB3-Laser (final tumor volume: 594.0 ± 45.8 mm^3; $p < 0.001$), demonstrating the advantages of NET-targeted drug delivery using KE108 as the targeting ligand. Key findings from the in vivo anticancer studies are summarized in Figure 7B. Taken together, AB3-loaded NIR-activated UCNP-based micelles conjugated with RB and KE108 (i.e., T-RB-AB3-Laser), which enabled NET-targeted combination chemotherapy and PDT, induced the best antitumor efficacy and did not cause any significant changes in body weight (Figure 7C) or survival. In addition, pathological assessment of hematoxylin and eosin (H&E)-stained sections of different organs (liver, brain, heart, and leg muscles) of mice treated with T-RB-AB3-Laser did not show any signs of acute or chronic inflammation, or apoptotic or necrotic regions (Figure 7D), thus suggesting that the UCNP-based theranostic micelles are safe for organs other than cancerous tissues.

3. Conclusions

An NET-targeted UCNP-based theranostic micelle was developed for simultaneous combination chemotherapy and PDT, as well as bioimaging, under NIR light illumination. The UCNP-based micelles exhibited excellent imaging capabilities both in vitro and in vivo.

The KE108 targeting ligand was capable of significantly enhancing the cellular and tumoral uptake of the micelles. Moreover, the NIR light effectively triggered fast drug release at the tumor sites, thereby achieving superior chemotherapy efficacy, and effectively generated cytotoxic $^1O_2$ for PDT. In vivo studies demonstrated that AB3-loaded UCNP-based micelles conjugated with both RB and KE108, capable of targeted combination chemotherapy and PDT, induced a dramatically better antitumor efficacy compared to chemotherapy or PDT alone, without any apparent systemic toxicity. Thus, this unique UCNP-based theranostic micelle could be a promising nanoplatform for targeted NET theranostics.

4. Experimental Section

Materials—CF_3CO_2Na, $Y(CF_3CO_2)_3$, $Yb(CF_3CO_2)_3$, $Tm(CF_3CO_2)_3$, and $Er(CF_3CO_2)_3$ were purchased from Rare Earth Products, Inc. (Beverly, MA, USA). AEP, RB, and DBCO were obtained from Sigma-Aldrich (St. Louis, MO, USA). Methoxy-PEG-OH (OCH_3-PEG-OH, M_n = 5 kDa) and OH-PEG-*N*-hydroxysuccinimide (HO-PEG-NHS, M_n = 5 kDa) were purchased from JenKem Technology (Allen, TX, USA). KE108 was purchased from Bachem Americas, Inc. (Torrance, CA, USA). All other agents were purchased from Fisher Scientific (Fitchburg, WI, USA) and used as received unless otherwise stated.

Synthesis of Amino-Functionalized $NaYF_4$:Yb^{3+}/Er^{3+}/Tm^{3+} UCNPs (NH_2-UCNPs)—The $NaYF_4$:Yb^{3+}/Er^{3+}/Tm^{3+} UCNP core was prepared using a thermal decomposition method.[12b] First, a three-neck round-bottom flask containing a magnetic stir bar was charged with CF_3CO_2Na (2 mmol), $Y(CF_3CO_2)_3$ (0.78 mmol), $Yb(CF_3CO_2)_3$ (0.2 mmol), $Tm(CF_3CO_2)_3$ (0.02 mmol), $Er(CF_3CO_2)_3$ (0.002 mmol), and oleylamine (12 mL). The solution was magnetically stirred and heated slowly to 120 °C under vacuum for 1 h to form the lanthanide oleate complexes, and to remove any residual acetic acid, water, and oxygen. The temperature was then increased to 320 °C as quickly as possible and this temperature was maintained for 1 h under an argon atmosphere. The mixture was then allowed to cool down to 80 °C. The UCNPs were precipitated by the addition of ethanol and isolated via centrifugation at 2000 rpm. The resulting pellets were dispersed in chloroform and precipitated with excess anhydrous ethanol. The UCNPs were isolated via centrifugation at 2000 rpm and then dispersed in chloroform for subsequent experiments.

In order to obtain NH_2-UCNPs, a ligand exchange method was adopted to transform the hydrophobic $NaYF_4$:Yb^{3+}/Er^{3+}/Tm^{3+} UCNPs into hydrophilic ones. Briefly, AEP (200 mg) was dissolved in a mixture of deionized (DI) water and ethanol (3:2, v/v, 10 mL). The UCNPs (20 mg) in chloroform (5 mL) were then added dropwise to the AEP solution and stirred vigorously using a magnetic stirring bar over 48 h at room temperature. After ligand exchange, the NH_2-UCNPs were collected via centrifugation at 2000 rpm and redispersed in 5 mL of water.

Synthesis of Rose Bengal Hexanoic Acid (RB-Acid)—The photosensitizer, RB, was reacted with 6-bromohexanoic acid in acetone/water (7:3, v/v) at 75 °C for 24 h. Thereafter, acetone was removed under vacuum. After three repetitions of liquid–liquid extraction in water and ethyl acetate, the RB-acid aqueous solution was collected and dried under lyophilization.

Synthesis of RB and Alkyne-Functionalized UCNPs—2 mg of NH_2-UCNPs, DBCO (3.14 mg), and RB-acid (6.3 mg) were dissolved in dimethyl sulfoxide (DMSO) and stirred vigorously over 48 h at room temperature. The impurities were then removed by dialysis against DI water for 48 h using a cellulose membrane (molecular weight cut-off, 8 kDa). The RB/alkyne-UNPCs were obtained after lyophilization. The alkyne-UCNPs (without RB conjugation) were prepared following a similar method.

Synthesis of 4,5-Dimethoxy-2-nitrobenzyl methacrylate (NBMA)—4,5-Dimethoxyl-2-nitrobenzyl alcohol (596 mg) and triethylamine (TEA, 1.97 mg) were dissolved in dichloromethane (10 mL). Methacryloyl chloride (0.4 mL, purified by distillation under vacuum before use) in 4 mL dichloromethane was added slowly to the above solution over 30 min through an addition funnel. After 3 h of reaction in an ice bath, the whole system was kept at room temperature overnight. After the removal of the solvent by a rotary evaporator, the crude product was dissolved in chloroform and purified by washing with HCl (1 M) and KCl (1 M) in sequence. Anhydrous $MgSO_4$ was used as a drying agent to absorb residual water. After filtration using a Büchner funnel, the solution was concentrated into a solid using a rotary evaporator and dried under vacuum overnight.

Synthesis of PEG-Br Macroinitiator—OCH_3-PEG-OH (50 mg) and TEA (2.25 mg) were dissolved in dry dichloromethane (10 mL) and stirred in an ice bath. 2-Bromoisobutyryl bromide (2.76 mg) in dichloromethane (5 mL) was added dropwise into this solution over 1 h. Next, the solution was stirred at room temperature overnight and then precipitated in cold ethyl ether. The crude product was purified by dissolving it in hot 2-propanol (70 °C) and precipitating it in cold 2-propanol. The polymer was then dried under vacuum. KE108-PEG-Br macroinitiator was synthesized following a similar method using KE108-PEG-OH instead. KE108-PEG-OH was synthesized by reacting KE108-NH_2 with NHS-PEG-OH at room temperature for 24 h.

Synthesis of PEG-PNBMA by ATRP—OCH_3-PEG-Br (0.009 mmol), NBMA (0.9 mmol), Cu(I)Br (0.018 mmol), and *N*,*N*,*N*′,*N*″,*N*″-pentamethyldiethylenetriamine (0.036 mmol) were dissolved in 1 mL DMSO. The mixture was degassed three times using a freeze–pump–thaw procedure, sealed under vacuum, and stirred in an oil bath (90 °C) for 13 h. The solution was then precipitated into methanol. The crude product was collected by filtration using a Büchner funnel and was purified by dissolving it in tetrahydrofuran (THF, 2 mL) and passing it through a neutral Al_2O_3 column with THF as an eluent solvent to remove any excess catalyst. The yellow filtrate was concentrated under a reduced pressure and reprecipitated twice into cold diethyl ether. The polymer was collected by centrifugation and dried under vacuum overnight. KE108-PEG-PNBMA was prepared following a similar method using KE108-PEG-Br as the macroinitiator.

Synthesis of PEG-PNBMA-N_3—PNBMA-PEG (20 mg) and NaN_3 (0.32 mg) were dissolved in DMSO (1.2 mL) and stirred for 48 h at 80 °C. The impurities were removed by dialysis against DI water for 48 h using a cellulose membrane (molecular weight cut-off, 8 kDa). The polymer was then dried under lyophilization.

Synthesis of UCNP-RB/PNBMA-PEG-OCH_3 (Abbreviated as UCNP-RB/PNBMA-PEG, Used to Prepare Nontargeted UCNP-Based Theranostic Micelles)— OCH_3-PEG-PNBMA-N_3 (10 mg) and UCNP-RB/alkyne (1 mg) were dissolved in DMSO (2 mL) and stirred for 48 h at room temperature. The impurities were removed by dialysis against DI water using a cellulose membrane (molecular weight cut-off, 15 kDa) for 48 h. The polymer was obtained under lyophilization. The UCNP-PNBMA-PEG-OCH_3 was prepared following a similar method using alkyne-UCNPs instead.

Synthesis of UCNP-RB/PNBMA-PEG-OCH_3/KE108 (Abbreviated as UCNP-RB/PNBMA-PEG-KE108, Used to Prepare Targeted UCNP-Based Theranostic Micelles)— OCH_3-PEG-PNBMA-N_3 (8.5 mg), KE108-PEG-PNBMA-N_3 (1.5 mg), and UCNP-RB/alkyne (1 mg) were dissolved in 2 mL DMSO and stirred for 48 h at room temperature. The impurities were removed by dialysis against DI water using a cellulose membrane (molecular weight cut-off, 15 kDa) for 48 h. The polymer was obtained under lyophilization. The UCNP-PNBMA-PEG-OCH_3/KE108 was prepared following a similar method using alkyne-UCNPs instead.

Synthesis of AB3-Loaded UCNP-RB/PNBMA-PEG-KE108 Theranostic Micelles (AB3-Loaded Theranostic Micelles)— To prepare AB3-loaded targeted theranostic micelles, AB3 (1.5 mg) and UCNP-RB/PNBMA-PEG-OCH_3/KE108 (5 mg) (i.e., T-RB-AB3) or UCNP-PNBMA-PEG-OCH_3/KE108 (5 mg) (i.e., T-AB3) were dissolved in 1 mL of dimethylformamide (DMF). DI water (3 mL) was added dropwise into the above solution. After another 2 h of stirring, the solution was dialyzed against DI water for 48 h. The final product was obtained by lyophilization. The AB3-loaded nontargeted theranostic micelles were prepared following a similar method using UCNP-RB/PNBMA-PEG-OCH_3 (i.e., NT-RB-AB3) or UCNP-PNBMA-PEG-OCH_3 (i.e., NT-AB3) instead.

Characterization— ^{1}H NMR spectra were recorded on a Varian Mercury Plus 300 spectrometer using DMSO-d_6, D_2O, or $CDCl_3$ as a solvent at 25 °C. FTIR spectra were recorded on a Bruker Tensor 27 FT-IR spectrometer. Molecular weights (M_n and M_w) and polydispersity indices (PDI; M_n/M_w) of the polymers were determined by gel permeation chromatography (GPC) equipped with triple detectors (i.e., a refractive index detector, a light scattering detector, and a viscometer detector) (Viscotek, USA) using DMF with 0.1 mmol of LiBr as a mobile phase. The luminescence spectrum of the UCNPs was acquired on a Nanolog FL3-2iHR spectrofluorometer (HORIBA Jobin Yvon, Inc., USA). The elemental analyses of the UCNPs were carried out using a scanning electron microscope (SEM, LEO GEMINI 1530, Zeiss, USA) equipped with EDX spectroscopy. The XRD pattern of the UCNPs was collected on a D8 Discover diffractometer (Bruker, USA). The morphologies of the UCNPs or UCNP-based micelles were determined by TEM (FEI Tecnai G2 F30 TWIN 300 kV, E.A. Fischione Instruments, Inc., USA) and DLS (ZetaSizer Nano ZS90, Malvern Instrument, USA). The AB3 and RB loading level (weight percentage) were measured by a Cary 500 UV-vis–NIR spectrophotometer based on a standard calibration curve for AB3 and RB at 297 and 560 nm, respectively.

NIR-Triggered PNBMA Hydrophobic-to-Hydrophilic Transition—^{1}H NMR analyses were performed to study the NIR-triggered hydrophobic-to-hydrophilic transition behavior of the PNBMA hydrophobic segments. In order to study the changes in the chemical structure of the PNBMA segments in the UCNP-PNBMA-PEG nanoparticles induced by NIR irradiation, 5 mg of UCNP-PNBMA-PEG was dispersed in 10 mL DI water and the resulting micelle solution then irradiated with a 980 nm laser (0.5 W cm^{-2}) for 10 min. The NIR-irradiated UCNP-PNBMA-PEG in the aqueous solution was collected by freeze-drying. To purify the NIR-irradiated UCNP-PNBMA-PEG, the resulting freeze-dried powder was first dissolved in DMSO and then precipitated in cold diethyl ether, which was subsequently dried under vacuum. ^{1}H NMR spectra of the UCNP-PNBMA-PEG polymer before and after 10 min 980 nm laser illumination (0.5 W cm^{-2}) were collected in DMSO-d_6.

NIR-Light Triggered $^1O_2$ Generation—DPBF is a commonly used agent to detect $^1O_2$.[26] As is typical, 20 μL of a DPBF/ethanol solution (10 mmol L^{-1}) was added to 2 mL of a solution containing either free RB or UCNP-based micelles with or without RB conjugation. The solution was kept in the dark and irradiated with a 980 nm laser (0.5 W cm^{-2}) for 16 min, and the absorption intensity of DPBF at 417 nm was recorded every 2 min. As the negative control groups, DPBF absorption in those three systems was also measured without 980 nm laser irradiation.

NIR-Light Triggered In Vitro Drug Release Profile—Drug release studies were performed in PBS solution at 37 °C. A 5 mL solution of AB3-loaded UCNP-based micelles was placed in a dialysis membrane (molecular weight cut-off 8 kDa), which was placed in 10 mL of release media. After 1 h incubation, the samples were irradiated with the 980 nm laser at an output power of 0.5 W cm^{-2} over a period of 10 min. At certain time points, 3 mL of media were collected and replaced by an equal amount of fresh media. The drug release behavior was monitored for 16 h. The amount of AB3 released was quantified by a UV–vis spectrophotometer at 297 nm. For the control group, the sample was kept in the dark without 980 nm irradiation throughout the experiment and the release media were collected at the same time points.

Cellular Uptake Study—The 650 nm luminescence band of the NIR (980 nm)-activated UCNPs was conveniently used for fluorescence imaging to study the effect of the KE108 peptide on the cellular uptake of the micelles in vitro using a multiphoton microscope with excitation and emission wavelengths of 980 and 650 nm, respectively. TT cells (human medullary thyroid cancer cell line; 1.4×10^4 cells cm^{-2}) were seeded in the eight-slide chamber and incubated overnight. Cells were then treated with KE108-conjugated UCNP-based micelles (i.e., targeted micelles) and nontargeted UCNP-based micelles (i.e., without KE108 conjugation) at a micelle concentration of 166 μg mL^{-1}. The blocking experiment with the coincubation of free KE108 (2×10^{-6} M) and targeted micelles was also performed. Cells treated with pure media were used as the control. After 2 h incubation, cells were washed with DPBS and fixed by 4% PFA. Thereafter, DAPI (2 μg mL^{-1}) was used to stain the cell nuclei. The sample was then subjected to multiphoton imaging with a Zeiss 20×/1.0 NA objective (see below).

Multiphoton Imaging—All multiphoton microscopy in this study was performed on an upright Ultima IV microscope (Bruker Nano Surfaces, Middleton, WI). An Insight DeepSee ultrafast Ti:Sapphire laser (Spectra Physics, Palo Alto, CA), tuned to 980 nm and directed through a Pockel's cell (ConOptics, Danbury, CT), was used for sample excitation. Fluorescence emission was split using a 445 nm dichroic and subsequently filtered through either a 620/60 BP filter (Chroma) for UCNP-based micelle emission (650 nm) or a 445/40 BP filter (Chroma) for DAPI emission. Fluorescence was then detected via multialkali photomultiplier tubes (Hamamatsu, Hamamatsu, Japan). Data were acquired using PrairieView software (Bruker Nano Surfaces, Middleton, WI).

In Vitro Cytotoxicity Evaluation—The in vitro cytotoxicity of UCNP-based micelles against TT cells was analyzed by MTT assay. Cells (8×10^4 cells cm^{-2}) were seeded into a 96-well plate and incubated overnight. The media were replaced with fresh media, or fresh media containing free AB3, free RB, a combination of free AB3 and RB, blank UCNP-based micelles (both targeted and nontargeted), AB3-loaded UCNP-based micelles (both targeted and nontargeted), RB-conjugated UCNP-based micelles (both targeted and nontargeted), or AB3-loaded and RB-conjugated UCNP-based micelles (both targeted and nontargeted) at an equivalent AB3 concentration of 2×10^{-6} M. After 3 h incubation, cells were irradiated by the 980 nm laser at a power density of 0.5 W cm^{-2} for 10 min. The cells were then incubated at 37 °C for another 45 h before applying the MTT reagent. The same panels were carried out for 48 h without laser treatment. Thereafter, a standard MTT protocol was carried out and cell viabilities (percentage of the pure media group without 980 nm laser illumination) were calculated.

In Vivo Tumoral Uptake of the Micelles—The 650 nm luminescence band of the NIR (980 nm)-activated UCNPs was utilized for in vivo fluorescence imaging. Male athymic nude mice (four week old) were purchased from Charles River (Wilmington, Maryland, USA).

A subcutaneous TT-tumor xenograft mouse model was established by the subcutaneous injection of 200 μL of Hanks balanced salt solution (Mediatech, Inc., Manassas, VA, USA) containing 1×10^7 of TT cells into the left flank. 10 d after inoculation, tumors of 5–6 mm in diameter were observed and TT-tumor-bearing mice were randomly divided into three groups (5 mice/group). The mice were intravenously injected with 200 μL of either saline (control), nontargeted micelles, or targeted micelles at a micelle concentration of 18.7 mg mL^{-1}. 5 h postinjection, the mice were scanned using a multiphoton microscope and an Olympus 4×/0.1 NA objective (see above). Excitation and emission wavelengths were 980 nm and 650 nm, respectively.

The tumor targeting ability of the micelles was also assessed in a NET liver metastases xenograft mouse model. In order to create NET liver metastases, each animal was anesthetized and placed on its right side. A small incision was then made in the left flank. The spleen was located and was further exposed and isolated with the aid of a tip applicator. About 5×10^6 TT cells (200 μL) were injected into the distal part of the spleen using a 25 G needle. 2 min postinjection, namely, after the TT cells entered into circulation, the splenic vessels were tied off and the spleen removed in order to decrease the ultimate tumor burden.

The skin and fascia were reapproximated with a vicryl suture. The mouse was then recovered from anesthesia, and the tumors were allowed to propagate. After confirmation of tumor progression by microCT scans (six weeks after cell injection), mice with liver metastases were treated with targeted UCNP-based micelles (18.7 mg mL^{-1}) via intravenous injection. The livers with tumor metastases were collected 7 h postinjection and images were taken using a fluorescence microscope with 980 nm excitation. Emission from the theranostic micelles at 650 nm was then detected in the liver.

In Vivo Anticancer Study—The same subcutaneous TT-tumor xenograft mouse model was used for the in vivo anticancer study. Mice were intravenously treated with ten groups (six mice per group) including: (1) saline (control); (2) free AB3; (3) AB3-loaded targeted micelles (T-AB3); (4) AB3-loaded targeted micelles with 980 nm laser illumination (T-AB3-Laser); (5) RB-conjugated targeted micelles (T-RB); (6) RB-conjugated targeted micelles with 980 nm laser illumination (T-RB-Laser); (7) AB3-loaded RB-conjugated nontargeted micelles (NT-RB-AB3); (8) AB3-loaded RB-conjugated nontargeted micelles with 980 nm laser illumination (NT-RB-AB3-Laser); (9) AB3-loaded RB-conjugated targeted micelles (T-RB-AB3); and (10) AB3-loaded RB-conjugated targeted micelles with 980 nm laser illumination (T-RB-AB3-Laser). The dosage of AB3 was 30 mg kg^{-1} BW. The dosage of AB3-loaded UCNP-based micelles (AB3 loading level was 16.7 wt%) in groups (7), (8), (9), and (10) was 180 mg kg^{-1} BW, corresponding to 30 mg kg^{-1} BW of AB3. The dosage of RB-conjugated UCNP-based micelles (without AB3 encapsulation) in groups (5) and (6) was 150 mg kg^{-1} BW. Each treatment group received two intravenous injections 7 d apart. For all treatment groups involving 980 nm laser treatment, a continuous wave fiber-coupled 980 nm laser (0.5 W cm^{-2}, 15 min, 1 min interval after every 5 min of irradiation) was applied at the tumor sites 4 h postinjection. Tumor volumes were measured with a caliper and then calculated using the formula: tumor volume = (length × $width^2$)/2. The weights of the mice were monitored during the experiment. At the end of the experiment, mice were sacrificed and a pathological examination of the lungs, heart, liver, and spleen was performed to confirm that there was no evidence of metastases or tumor growth outside of the inoculation sites. All major organs of the mice treated with T-AB3-RB-Laser, including the liver, brain, heart, and leg muscles, were collected, and H&E-stained sections were prepared for pathological assessment. All experimental procedures were carried out in compliance with our animal care protocol, which was approved by the Animal Care and Use Committee at the University of Wisconsin–Madison.

Supplementary Material

Refer to Web version on PubMed Central for supplementary material.

Acknowledgments

G.C. and R.J.-S. contributed equally to this work. This project was financially supported by grants from the NIH (K25CA166178 and R21CA196653 to S. Gong, and R01 CA121115 to H. Chen), the Aly Wolff Memorial Foundation (S. Gong and H. Chen), the American Cancer Society (MEN2 Thyroid Cancer Professorship 120319-RPM-11-080-01–TBG to H. Chen and Research Scholar Award RSGM TBE-121413 to H. Chen). The authors would also like to express their appreciation to Prof. Weibo Cai at the University of Wisconsin–Madison for providing the NIR-laser instrument for our studies, and Dr. Feng Chen for the helpful discussion related to the synthesis and characterization of UCNPs.

References

1. a) Adler JT, Meyer-Rochow GY, Chen H, Benn DE, Robinson BG, Sippel RS, Sidhu SB. Oncologist. 2008; 13:779. [PubMed: 18617683] b) Pinchot SN, Pitt SC, Sippel RS, Kunnimalaiyaan M, Chen H. Curr Opin Invest Drugs. 2008; 9:576.c) Chen H, Hardacre JM, Uzar A, Cameron JL, Choti MA. J Am Coll Surg. 1998; 187:88. [PubMed: 9660030] d) Chen H, Pruitt A, Nicol TL, Gorgulu S, Choti MA. J Gastrointest Surg. 1998; 2:151. [PubMed: 9834411] e) Chen H. J Surg Oncol. 2008; 97:203. [PubMed: 18264978]
2. Norton JA. Best Pract Res, Clin Gastroenterol. 2005; 19:577. [PubMed: 16183528]
3. a) Brown KT, Koh BY, Brody LA, Getrajdman GI, Susman J, Fong Y, Blumgart LH. J Vasc Interv Radiol. 1999; 10:397. [PubMed: 10229465] b) Miller CA, Ellison EC. Surg Oncol Clin North Am. 1998; 7:863.
4. a) Isozaki T, Kiba T, Numata K, Saito S, Shimamura T, Kitamura T, Morita K, Tanaka K, Sekihara H. Int Med. 1999; 38:17.b) Eriksson B, Kloppel G, Krenning E, Ahlman H, Plockinger U, Wiedenmann B, Arnold R, Auernhammer C, Korner M, Rindi G, Wildi S. Neuroendocrinology. 2008; 87:8. [PubMed: 18097129] c) Lal A, Chen H. Curr Opin Oncol. 2006; 18:9. [PubMed: 16357558] d) Lehnert T. Transplantation. 1998; 66:1307. [PubMed: 9846513] e) Zhang R, Straus FH, DeGroot LJ. Endocrinology. 1999; 140:2152. [PubMed: 10218966] f) Boudreaux JP, Putty B, Frey DJ, Woltering E, Anthony L, Daly I, Ramcharan T, Lopera J, Castaneda W. Ann Surg. 2005; 241:839. [PubMed: 15912033] g) Nguyen C, Faraggi M, Giraudet AL, de Labriolle-Vaylet C, Aparicio T, Rouzet F, Mignon M, Askienazy S, Sobhani I. J Nucl Med. 2004; 45:1660. [PubMed: 15471830] h) Fiorentini G, Rossi S, Bonechi F, Vaira M, De Simone M, Dentico P, Bernardeschi P, Cantore M, Guadagni S. J Chemother. 2004; 16:293. [PubMed: 15330328] i) Zuetenhorst JM, Olmos RAV, Muller M, Hoefnagel CA, Taal BG. Endocr-Relat Cancer. 2004; 11:553. [PubMed: 15369454]
5. a) Xu W, Siddiqui IA, Nihal M, Pilla S, Rosenthal K, Mukhtar H, Gong S. Biomaterials. 2013; 34:5244. [PubMed: 23582862] b) Yang X, Grailer JJ, Pilla S, Steeber DA, Gong S. Bioconjugate Chem. 2010; 21:496.c) Guo J, Hong H, Chen G, Shi S, Nayak TR, Theuer CP, Barnhart TE, Cai W, Gong S. ACS Appl Mater Interfaces. 2014; 6:21769. [PubMed: 24628452] d) Peer D, Karp JM, Hong S, Farokhzad OC, Margalit R, Langer R. Nat Nanotechnol. 2007; 2:751. [PubMed: 18654426] e) Win KY, Feng SS. Biomaterials. 2005; 26:2713. [PubMed: 15585275] f) Shi X, Chen G, Guo LW, Si Y, Zhu M, Pilla S, Liu B, Gong S, Kent KC. PloS One. 2014; 9:e89227. [PubMed: 24586612]
6. a) Greish K. Methods Mol Biol. 2010; 624:25. [PubMed: 20217587] b) Reuveni T, Motiei M, Romman Z, Popovtzer A, Popovtzer R. Int J Nanomed. 2011; 6:e64.c) Ma J, Huang P, He M, Pan L, Zhou Z, Feng L, Gao G, Cui D. J Phys Chem B. 2012; 116:14062. [PubMed: 23134318] d) Bartlett DW, Su H, Hildebrandt IJ, Weber WA, Davis ME. Proc Natl Acad Sci USA. 2007; 104:15549. [PubMed: 17875985] e) Xiao Y, Hong H, Javadi A, Engle JW, Xu W, Yang Y, Zhang Y, Barnhart TE, Cai W, Gong S. Biomaterials. 2012; 33:3071. [PubMed: 22281424]
7. a) Fan W, Shen B, Bu W, Chen F, He Q, Zhao K, Zhang S, Zhou L, Peng W, Xiao Q, Ni D, Liu J, Shi J. Biomaterials. 2014; 35:8992. [PubMed: 25103233] b) Wang T, Zhang L, Su Z, Wang C, Liao Y, Fu Q. ACS Appl Mater Interfaces. 2011; 3:2479. [PubMed: 21604817] c) Kimura M, Miyajima K, Kojika M, Kono T, Kato H. Int J Mol Sci. 2015; 16:25466. [PubMed: 26512656] d) Colasanti A, Kisslinger A, Quarto M, Riccio P. Acta Biochim Pol. 2005; 51:1039.e) Ma M, Chen H, Chen Y, Wang X, Chen F, Cui X, Shi J. Biomaterials. 2012; 33:989. [PubMed: 22027594] f) Shiah JG, Sun Y, Kopečková P, Peterson C, Straight R, Kopeček J. J Controlled Release. 2001; 74:249.g) Khdair A, Chen D, Patil Y, Ma L, Dou QP, Shekhar MP, Panyam J. J Controlled Release. 2010; 141:137.
8. Agostinis P, Berg K, Cengel KA, Foster TH, Girotti AW, Gollnick SO, Hahn SM, Hamblin MR, Juzeniene A, Kessel D, Korbelik M, Moan J, Mroz P, Nowis D, Piette J, Wilson BC, Golab J. CA Cancer J Clin. 2011; 61:250. [PubMed: 21617154]
9. a) Dolmans D, Fukumura D, Jain R. Nat Rev Cancer. 2003; 3:380. [PubMed: 12724736] b) Castano AP, Mroz P, Hamblin MR. Nat Rev Cancer. 2006; 6:535. [PubMed: 16794636]
10. Juarranz Á, Jaén P, Sanz-Rodríguez F, Cuevas J, González S. Clin Transl Oncol. 2008; 10:148. [PubMed: 18321817]

11. a) Weissleder R, Ntziachristos V. Nat Med. 2003; 9:123. [PubMed: 12514725] b) Idris NM, Gnanasammandhan MK, Zhang J, Ho PC, Mahendran R, Zhang Y. Nat Med. 2012; 18:1580. [PubMed: 22983397] c) Cui S, Yin D, Chen Y, Di Y, Chen H, Ma Y, Achilefu S, Gu Y. ACS Nano. 2012; 7:676. [PubMed: 23252747]
12. a) Wang C, Tao H, Cheng L, Liu Z. Biomaterials. 2011; 32:6145. [PubMed: 21616529] b) Liu K, Liu X, Zeng Q, Zhang Y, Tu L, Liu T, Kong X, Wang Y, Cao F, Lambrechts S, Aalder M, Zhang H. ACS Nano. 2012; 6:4054. [PubMed: 22463487] c) Zhou L, Li Z, Liu Z, Yin M, Ren J, Qu X. Nanoscale. 2014; 6:1445. [PubMed: 24316678] d) Chen Z, Liu Z, Li Z, Ju E, Gao N, Zhou L, Ren J, Qu X. Biomaterials. 2015; 39:15. [PubMed: 25477167] e) Liu Z, Li Z, Liu J, Gu S, Yuan Q, Ren J, Qu X. Biomaterials. 2012; 33:6748. [PubMed: 22770569]
13. a) Idris NM, Gnanasammandhan MK, Zhang J, Ho PC, Mahendran R, Zhang Y. Nat Med. 2012; 18:1580. [PubMed: 22983397] b) Cheng L, Wang C, Liu Z. Nanoscale. 2013; 5:23. [PubMed: 23135546] c) Tian G, Zhang X, Gu Z, Zhao Y. Adv Mater. 2015; 27:7692. [PubMed: 26505885] d) Wang C, Cheng L, Liu Z. Theranostics. 2013; 3:317. [PubMed: 23650479] e) Wang Y, Liu K, Liu X, Dohnalová KI, Gregorkiewicz T, Kong X, Aalders MC, Buma WJ, Zhang H. J Phys Chem Lett. 2011; 2:2083.f) Ai F, Ju Q, Zhang X, Chen X, Wang F, Zhu G. Sci Rep. 2015; 5:10785. [PubMed: 26035527]
14. a) Shan J, Budijono SJ, Hu G, Yao N, Kang Y, Ju Y, Prud'homme RK. Adv Funct Mater. 2011; 21:2488.b) Huang P, Lin J, Wang S, Zhou Z, Li Z, Wang Z, Zhang C, Yue X, Niu G, Yang M. Biomaterials. 2013; 34:4643. [PubMed: 23523428]
15. Xia L, Kong X, Liu X, Tu L, Zhang Y, Chang Y, Liu K, Shen D, Zhao H, Zhang H. Biomaterials. 2014; 35:4146. [PubMed: 24529625]
16. a) Yin M, Ju E, Chen Z, Li Z, Ren J, Qu X. Chem - Eur J. 2014; 20:14012. [PubMed: 25200923] b) Zhang T, Lin H, Cui L, An N, Tong R, Chen Y, Yang C, Li X, Qu F. RSC Adv. 2016; 6:26479.c) Ai F, Sun T, Xu Z, Wang Z, Kong W, To MW, Wang F, Zhu G. Dalton Trans. 2016; 45:13052. [PubMed: 27430044] d) Yuan Y, Min Y, Hu Q, Xing B, Liu B. Nanoscale. 2014; 6:11259. [PubMed: 25130329] e) Yuan Y, Liu B. ACS Appl Mater Interfaces. 2014; 6:14903. [PubMed: 25075548] f) Yang S, Li N, Liu Z, Sha W, Chen D, Xu Q, Lu J. Nanoscale. 2014; 6:14903. [PubMed: 25362857] g) Fan W, Shen B, Bu W, Chen F, He Q, Zhao K, Zhang S, Zhou L, Peng W, Xiao Q. Biomaterials. 2014; 35:8992. [PubMed: 25103233] h) Yue C, Zhang C, Alfranca G, Yang Y, Jiang X, Yang Y, Pan F, de la Fuente JM, Cui D. Theranostics. 2016; 6:456. [PubMed: 26941840]
17. a) Chen Z, Zhang L, Sun Y, Hu J, Wang D. Adv Funct Mater. 2009; 19:3815.b) Wang Z, Li W, Yu N, Liu Z, Zhang L, Chen Z. RSC Adv. 2016; 6:42763.
18. Cui S, Yin D, Chen Y, Di Y, Chen HM, Achilefu YS, Gu Y. ACS Nano. 2013; 7:676. [PubMed: 23252747]
19. a) Cheng R, Meng F, Deng C, Klok HA, Zhong Z. Biomaterials. 2013; 34:3647. [PubMed: 23415642] b) Chytil P, Etrych T, Konak C, Sirova M, Mrkvan T, Boucek J, Rihova B, Ulbrich K. J Controlled Release. 2008; 127:121.c) Dai J, Lin S, Cheng D, Zou S, Shuai X. Angew Chem, Int Ed Engl. 2011; 50:9404. [PubMed: 21898731]
20. Chen G, Jaskula-Sztul R, Harrison A, Dammalapati A, Xu W, Cheng Y, Chen H, Gong S. Biomaterials. 2016; 97:22. [PubMed: 27156249]
21. Ning X, Guo J, Wolfert MA, Boons GJ. Angew Chem, Int Ed Engl. 2008; 47:2253. [PubMed: 18275058]
22. Redmond RW, Gamlin JN. Photochem Photobiol. 1999; 70:391. [PubMed: 10546544]
23. a) Guo J, Hong H, Chen G, Shi S, Zheng Q, Zhang Y, Theuer CP, Barnhart TE, Cai W, Gong S. Biomaterials. 2013; 34:8323. [PubMed: 23932288] b) Chen G, Wang L, Cordie T, Vokoun C, Eliceiri KW, Gong S. Biomaterials. 2015; 47:41. [PubMed: 25682159] c) Brinkman AM, Chen G, Wang Y, Hedman CJ, Sherer NM, Havighurst TC, Gong S, Xu W. Biomaterials. 2016; 101:20. [PubMed: 27267625]
24. a) Blanco E, Shen H, Ferrari M. Nat Biotechnol. 2015; 33:941. [PubMed: 26348965] b) Cabral H, Matsumoto Y, Mizuno K, Chen Q, Murakami M, Kimura M, Terada Y, Kano M, Miyazono K, Uesaka M. Nat Nanotechnol. 2011; 6:815. [PubMed: 22020122]

25. a) Jiang J, Tong X, Morris D, Zhao Y. Macromolecules. 2006; 39:4633.b) Wang Y, Han P, Xu H, Wang Z, Zhang X, Kabanov AV. Langmuir. 2009; 26:709.c) He J, Tong X, Zhao Y. Macromolecules. 2009; 42:4845.

26. Chen F, Zhang S, Bu W, Chen Y, Xiao Q, Liu J, Xing H, Zhou L, Peng W, Shi J. Chemistry. 2012; 18:7082. [PubMed: 22544381]

27. a) Jaskula-Sztul R, Xu W, Chen G, Harrison A, Dammalapati A, Nair R, Cheng Y, Gong S, Chen H. Biomaterials. 2016; 91:1. [PubMed: 26994874] b) Gabriel M, Decristoforo C, Kendler D, Dobrozemsky G, Heute D, Uprimny C, Kovacs P, von Guggenberg E, Bale R, Virgolini IJ. J Nucl Med. 2007; 48:508. [PubMed: 17401086]

28. a) Wang F, Banerjee D, Liu Y, Chen X, Liu X. Analyst. 2010; 135:1839. [PubMed: 20485777] b) Xiong L, Yang T, Yang Y, Xu C, Li F. Biomaterials. 2010; 31:7078. [PubMed: 20619791]

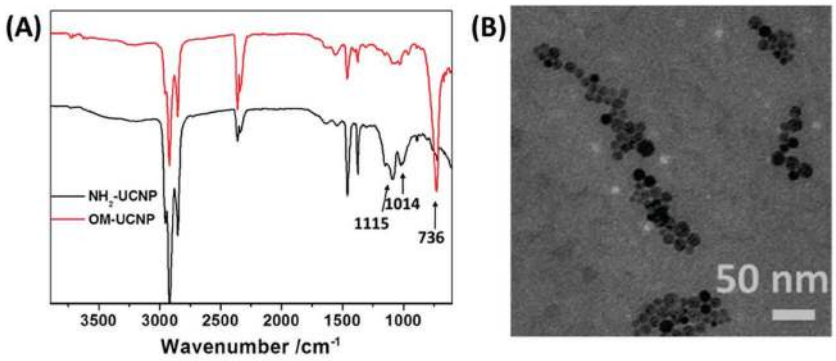

Figure 1.

A) FTIR absorption spectra of the oleylamine-stabilized UCNPs (OM-UCNP) (red curve) and NH_2-UCNPs (black curve). B) TEM image of the NH_2-UCNPs.

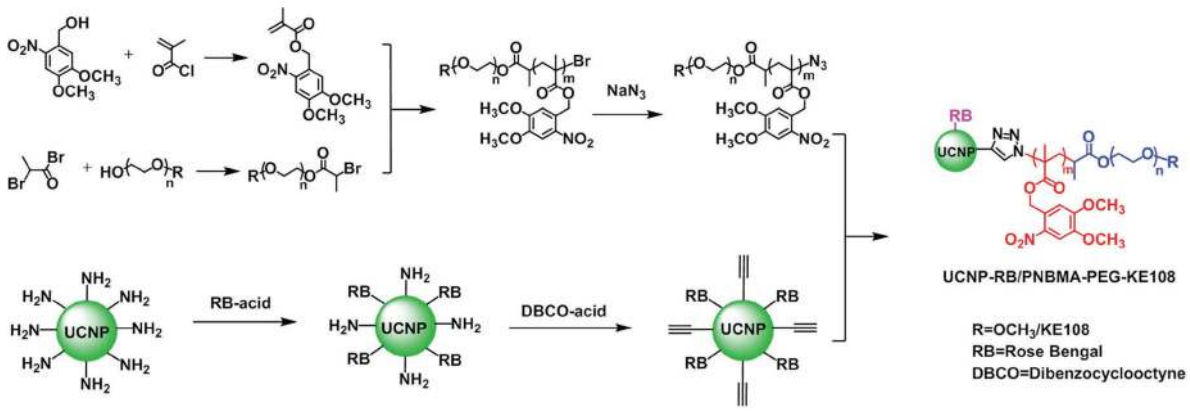

Figure 2.

Synthesis scheme of the multifunctional UCNP-based theranostic micelles (UCNP-RB/PNBMA-PEG-KE108).

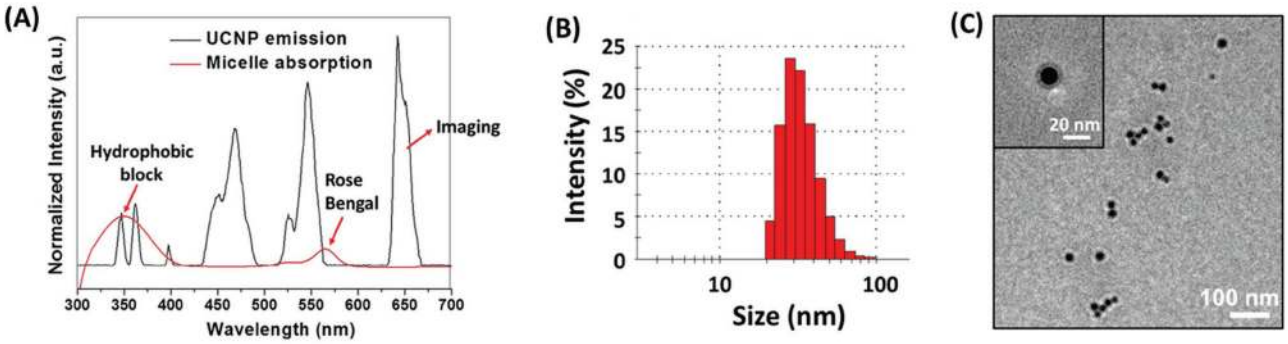

Figure 3.

A) Spectral overlap between the upconversion emission spectrum of the UCNPs (black curve) and the UV–vis absorption spectrum of the UCNP-based theranostic micelles (red curve). B) Dynamic light scattering (DLS) analyses and C) transmission electron microscopy (TEM) image of the UCNP-based theranostic micelles.

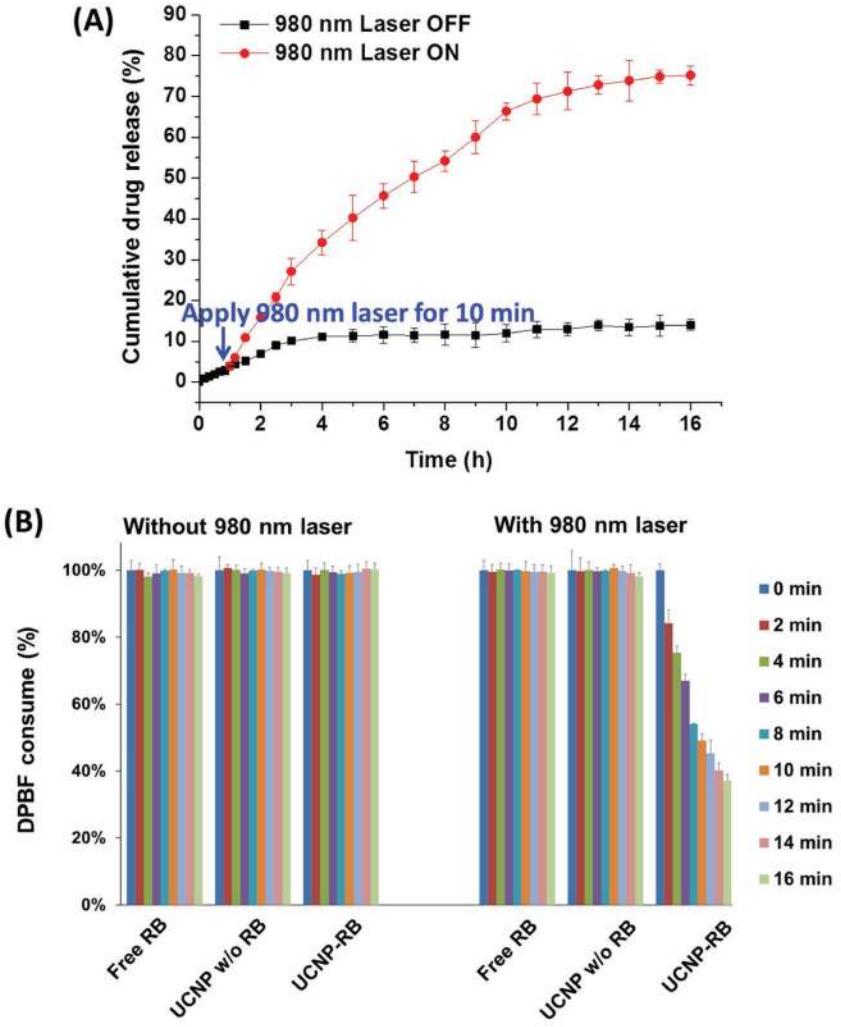

Figure 4.

NIR-triggered A) in vitro drug release profile and B) singlet oxygen ($^1O_2$) generation.

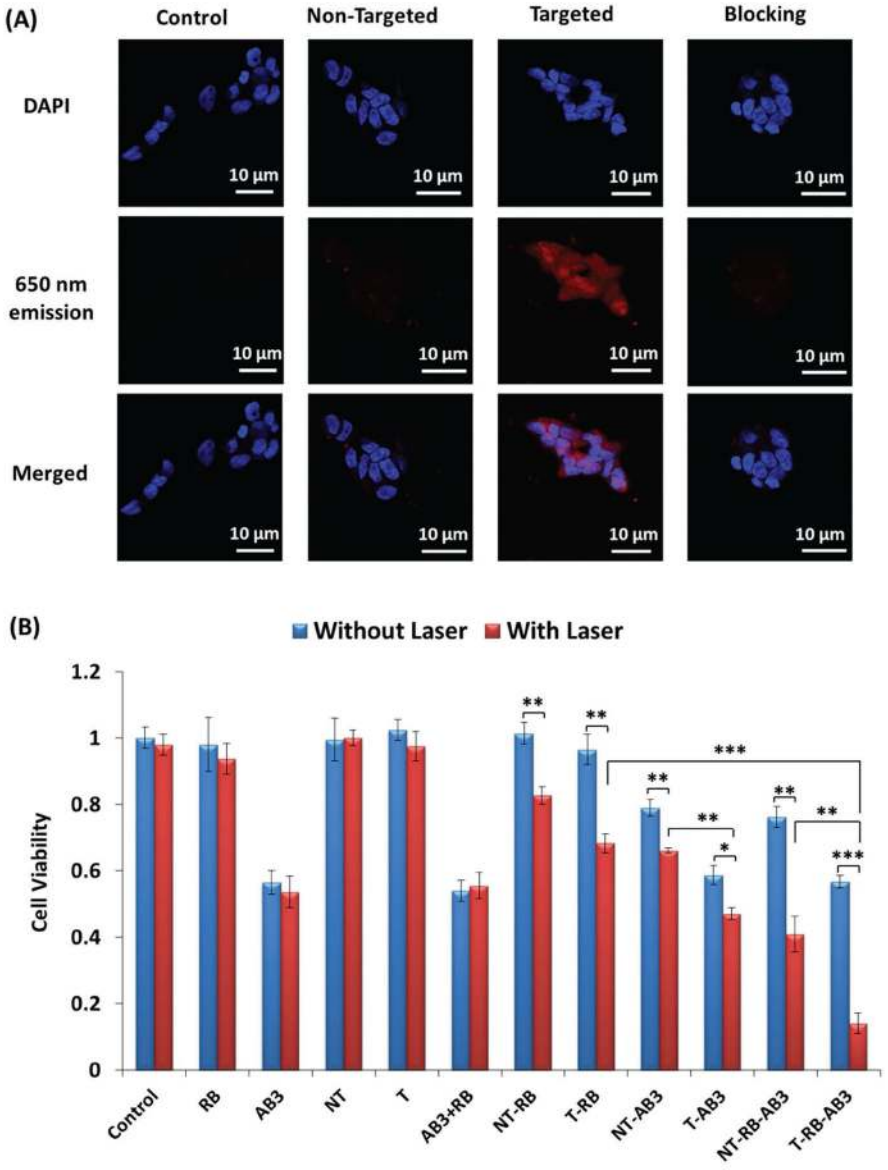

Figure 5.

A) In vitro cellular uptake study of the UCNP-based theranostic micelles in NET (TT) cells. Cells were treated with pure medium (i.e., control), nontargeted (i.e., lacking KE108) micelles, and targeted (i.e., KE108-conjugated) micelles (166 μg mL^{-1}), as well as the combination of free KE108 peptide (2×10^{-6} M) and targeted micelles (i.e., blocking) for 2 h at 37 °C. Images were taken under a multiphoton microscope based on the 650 nm luminescence emission of the NIR-activated UCNPs (Ex/Em: 980/650 nm). B) In vitro evaluation of cell viabilities. Abbreviation for all treatment groups was summarized in Table 1. For all laser-related treatments, the cells were first incubated with micelles for 3 h, followed by irradiation by the 980 nm laser at a power density of 0.5 W cm^{-2} for 10 min. The cells were then incubated at 37 °C for another 45 h. *: $p < 0.05$; **: $p < 0.01$; ***: $p < 0.001$.

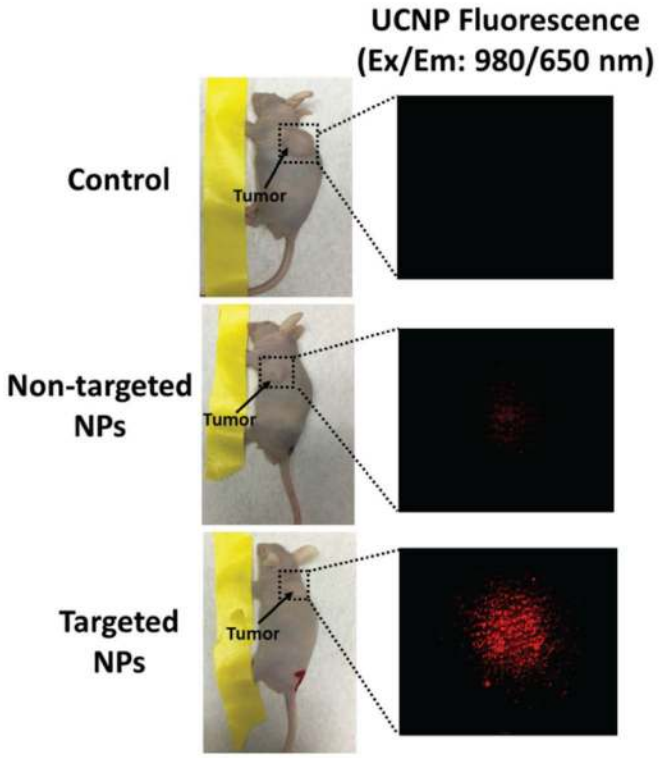

Figure 6.

Tumor accumulation of the UCNP-based theranostic micelles in TT-tumor-bearing mice. The mice were intravenously treated with saline (control), nontargeted micelles (i.e., UNCP-based micelles without KE108 conjugation), and targeted micelles (i.e., KE108-conjugated UCNP-based micelles). The mice were analyzed using a multiphoton microscope (Ex/Em: 980/650 nm) 5 h postinjection.

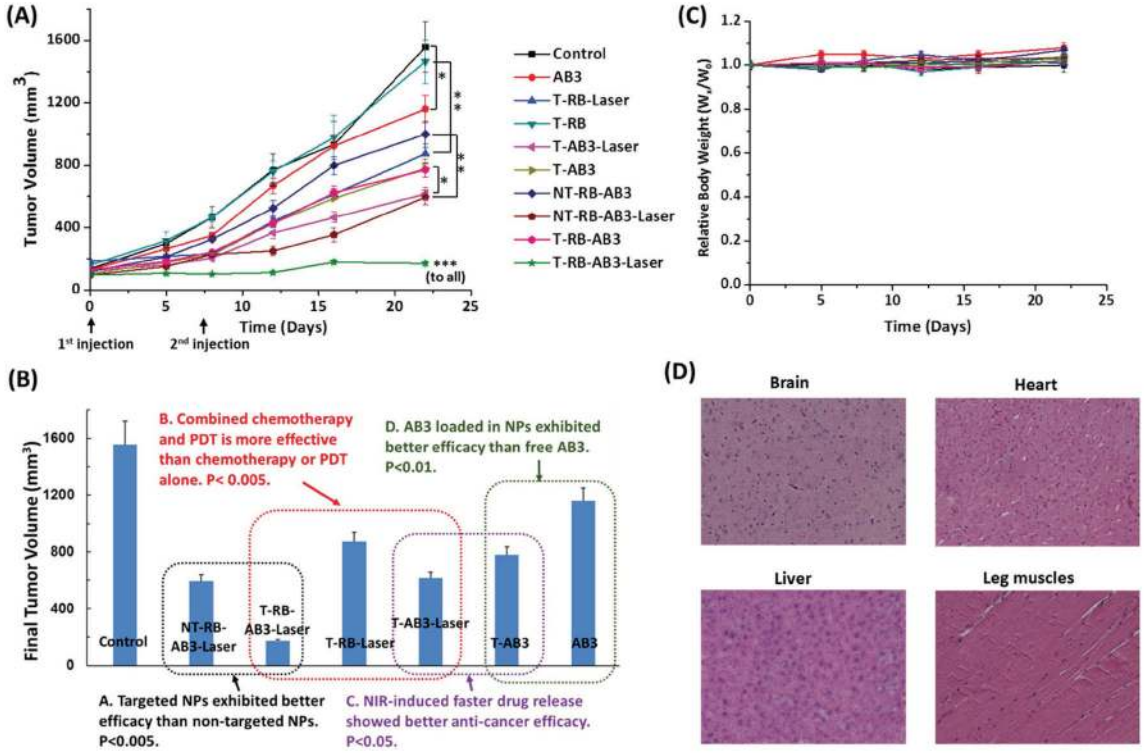

Figure 7.

A) In vivo anticancer efficacy of different formulations of UCNP-based theranostic micelles in NET xenografts. Tumor-bearing mice were treated with ten groups: (1) Saline (control); (2) AB3 (conventional chemotherapy); (3) T-RB (no PDT effect as no laser illumination); (4) T-RB-Laser (targeted NIR-controlled PDT); (5) T-AB3 (targeted chemotherapy); (6) T-AB3-Laser (targeted NIR-controlled chemotherapy); (7) NT-AB3-RB (nontargeted chemotherapy; no PDT effect as no laser illumination); (8) NT-AB3-RB-Laser (nontargeted combination NIR-controlled chemotherapy and PDT); (9) T-AB3-RB (targeted chemotherapy; no PDT effect as no laser illumination); and (10) T-AB3-RB-Laser (targeted combination NIR-controlled chemotherapy and PDT). Each mouse received two intravenous injections (30 mg kg^{-1} BW of AB3) over a 7 d interval. A continuous wave fiber-coupled 980 nm laser (0.5 W cm^{-2}, 15 min, 1 min interval after every 5 min of irradiation) was applied at the tumor sites in the "Laser" groups 4 h postinjection. B) The final tumor volumes and key findings for the anticancer study. C) Change in body weight of animals as a function of time. W_x: body weight at selected time point; W_0: initial body weight. D) Representative H&E-stained sections of the brain, heart, liver, and leg muscles of the mouse treated with T-RB-AB3-Laser micelles. No signs of apoptotic or necrotic areas were observed. All values are presented as a mean SD ($n = 6$). *: $p < 0.05$; **: $p < 0.01$; ***: $p < 0.001$.

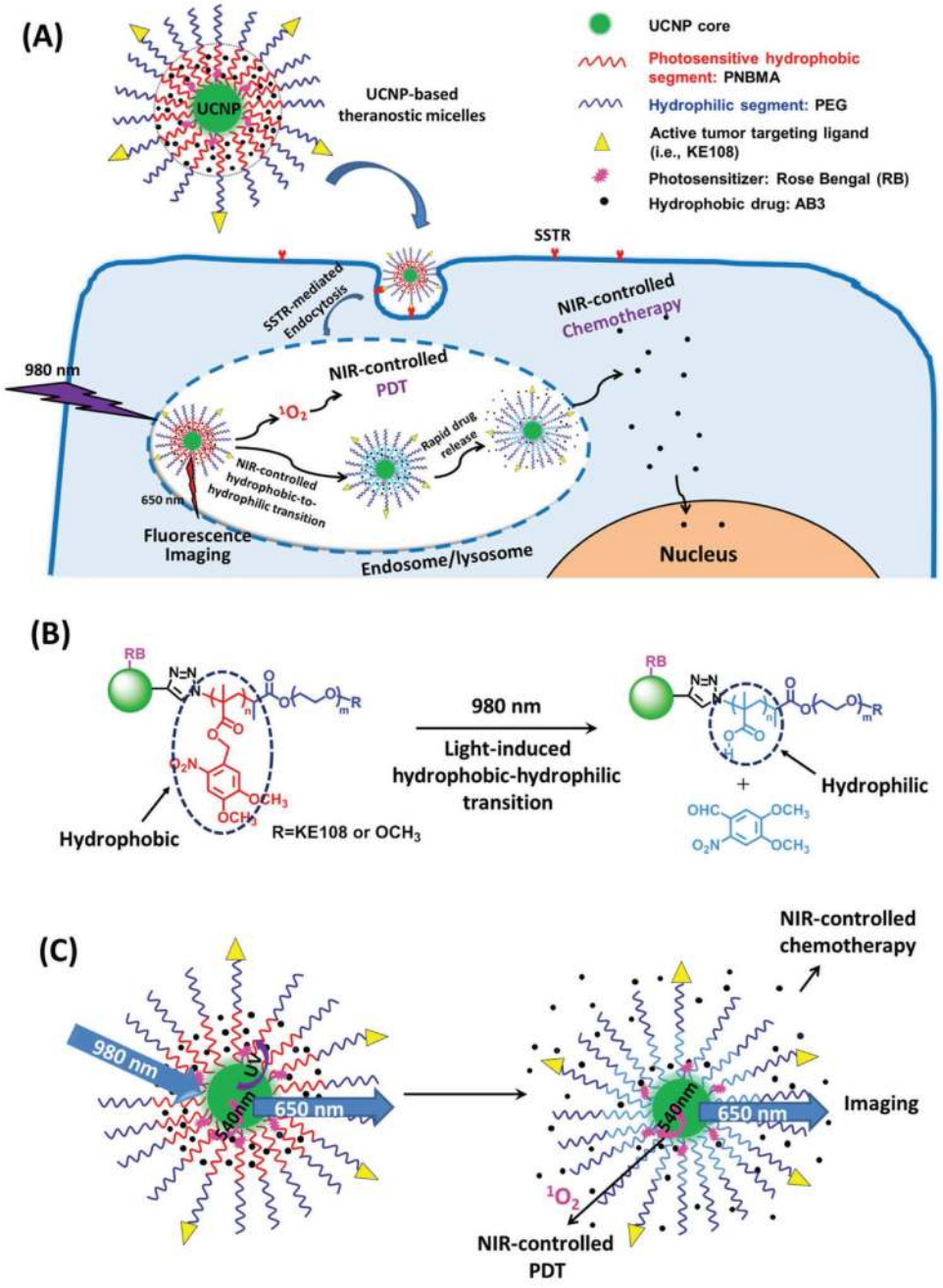

Scheme 1.

A) NET-targeted UCNP-based theranostic micelles for simultaneous NIR-controlled combination chemotherapy and PDT, as well as fluorescence imaging. B) An illustration of the NIR-triggered hydrophobic-to-hydrophilic transition. C) An illustration of NIR-controlled combination chemotherapy and PDT, as well as fluorescence imaging.

Table 1

Abbreviations for all treatment formulations.

Control	PBS (in vitro) or saline (in vivo)
AB3	Free AB3 (an HDAC inhibitor) without any carrier
RB	Free Rose Bengal (photosensitizer) without any carrier
NT	Blank UCNP-based nontargeted micelles
T	Blank UCNP-based targeted micelles
AB3 + RB	The combination of free AB3 and RB
NT-RB	RB-conjugated UCNP-based nontargeted micelles
NT-AB3	AB3-loaded UCNP-based nontargeted micelles
NT-RB-AB3	AB3-loaded and RB-conjugated UCNP-based nontargeted micelles
T-RB	RB-conjugated UCNP-based targeted (i.e., KE108-conjugated) micelles
T-AB3	RB-conjugated UCNP-based targeted NPs
T-RB-AB3	AB3-loaded and RB-conjugated UCNP-based targeted micelles